Dark Matter direct detection & Sub-10 ps ToF

Junhui LIAO

Brown University

outline

1. DM direct detection: "theoretical" stuff
   - The existence of DM
   - The strategies of DM detection
   - The key features of DM direct detection
   - Characterize DM signals in direct detection: SI / SD and EFT
2. DM direct detection: experimental stuff
   - Brief review of the experiments in the field
3. Low-mass ($\sim$ 1 - 10 GeV/c^2) WIMPs direct detection, DAMIC
   - DAMIC and CCD introduction
   - Detector calibration
   - Limits setting with SI and EFT for DAMIC
   - Summary for DAMIC
4. High-mass ($\sim$ 10 - 1000 GeV/c^2) WIMPs direct detection, LZ
   - LZ review
   - Brown's contribution to LZ: PMTs assembly
   - LXe calibration with mono-energetic 300 keV neutrons
5. Sub-10 ps ToF for CMS
   - A little detour to the LHC
   - GASTOF
   - GASTOF study

BROWN

outline

BROWN

Does DM exist ? Two interpretations !

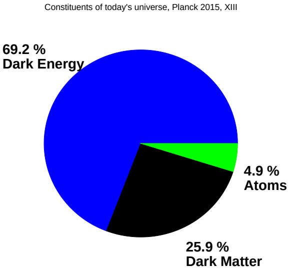

Velocities of galaxies in the M33 cluster.

Does DM exist ? Two interpretations !

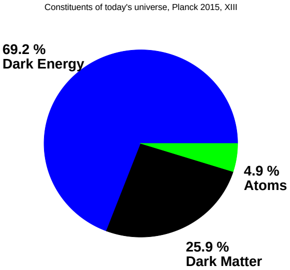

Velocities of galaxies in the M33 cluster.

Does DM exist ? Two interpretations !

Constituents of today's universe, Planck 2015, XIII

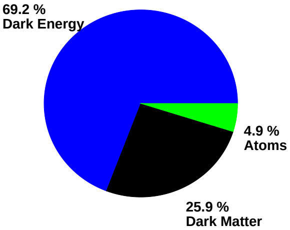

Velocities of galaxies in the M33 cluster.

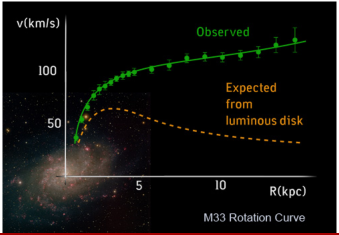

Does DM exist ? Two interpretations !

Constituents of today's universe, Planck 2015, XIII

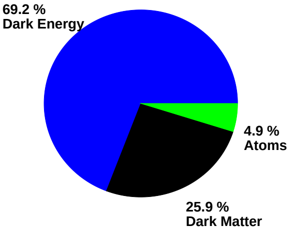

Velocities of galaxies in the M33 cluster.

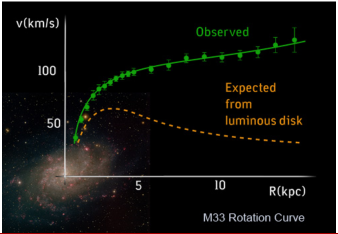

To interpret the discrepancy of velocities, $m\frac{v^2}{r} = ma \neq G\frac{mM}{r^2}$. Two proposed ideas:
Fritz Zwicky proposed more invisible matter - DM in 1930s;
Mordehai Milgrom proposed Modified Newtonian Dynamics (MOND) in 1980s, DM was not necessary.

BROWN

“Judgment Day”: 2016

Observations of Bullet Cluster

- Observations of two clusters passing through each other after a collision.
- Normal matter found from X-ray.
- Total matter from Gravitational lensing.
- Bullet results : TAJ, 648:L109-113, 2006. Contrary to MOND prediction.

The data “adjudged”: DM exists in the Bullet Cluster.

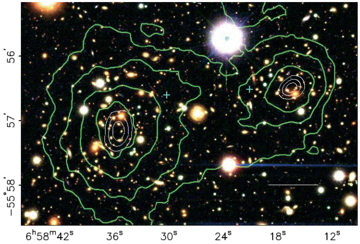

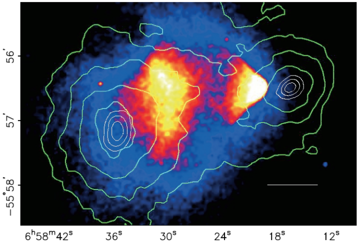

Other evidence of the existence of DM

CMB simulation and observation

- Left plot: Simulation of galaxies formation. DM has been added in the simulation; without DM, galaxies can not be formed like that.
- Right plot: temperature plot of CMB (Cosmic Microwave Background), Planck 2015 data. Temperature distribution $\rightarrow$ mass distribution $\rightarrow$ DM exists.

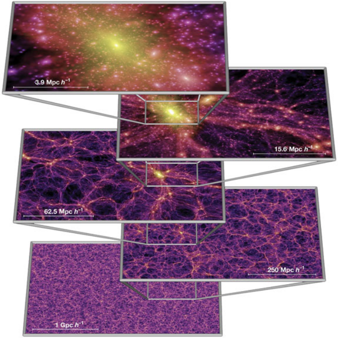

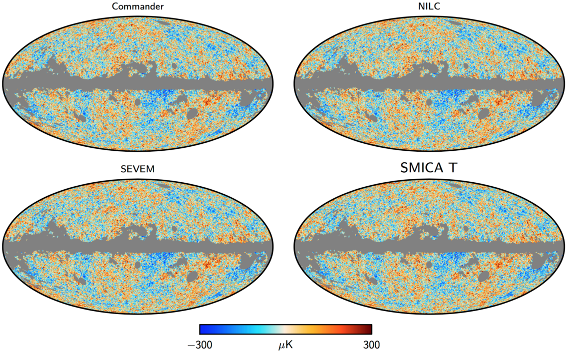

Most of physicists in the filed believe DM exists, very few doesn't

The debate of the existence of DM is still going on and on ...

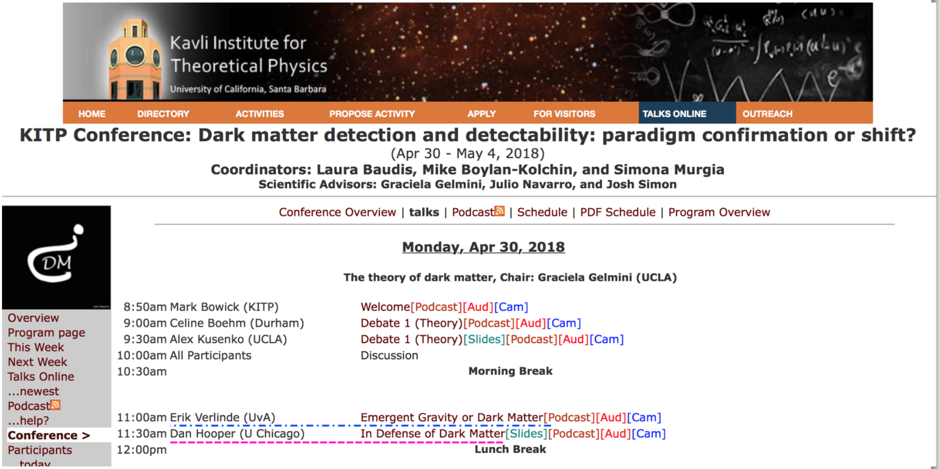

KITP Conference: Dark matter detection and detectability: paradigm confirmation or shift?

(Apr 30 - May 4, 2018)

Coordinators: Laura Baudis, Mike Boylan-Kolchin, and Simona Murgia

Scientific Advisors: Graciela Gelmini, Julio Navarro, and Josh Simon

Conference Overview | **talks** | Podcast | Schedule | PDF Schedule | Program Overview

Monday, Apr 30, 2018

The theory of dark matter, Chair: Graciela Gelmini (UCLA)

8:50am	Mark Bowick (KITP)	Welcome[Podcast][Aud][Cam]
9:00am	Celine Boehm (Durham)	Debate 1 (Theory)[Podcast][Aud][Cam]
9:30am	Alex Kusenko (UCLA)	Debate 1 (Theory)[Slides][Podcast][Aud][Cam]
10:00am	All Participants	Discussion
10:30am		**Morning Break**
11:00am	Erik Verlinde (UvA)	Emergent Gravity or Dark Matter[Podcast][Aud][Cam]
11:30am	Dan Hooper (U Chicago)	In Defense of Dark Matter[Slides][Podcast][Aud][Cam]
12:00pm		**Lunch Break**

outline

Understanding the nature of DM besides Gravitation

Strategies of DM searches with indirect detection: $\chi\chi \xrightarrow{annihilate}$ SM SM.

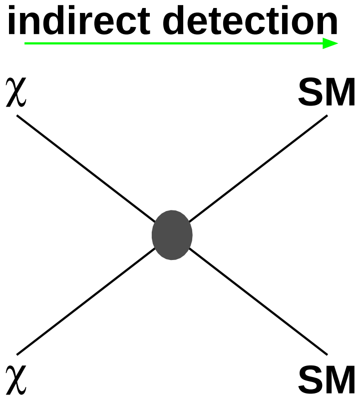

- $\chi\chi \to \nu$, from the Sun
  To measure: higher energy ν.
  Experiments: SuperK, IceCube.
  Status: no signal, limit $\sigma_A v \sim 10^{-23} cm^3 s^{-1}$
- $\chi\chi \to e^+e^-$, in galaxies
  To measure: excess of e^+.
  Experiments: AMS, Fermi-LAT, PAMELA, DAMPE (Wukong).
  Status: no signal. Hard to rule out Pulsars (AMS02 take data until 2030).
- $\chi\chi \to \gamma$, in Milky Way.
  To measure: excess of γ.
  Experiments: Fermi-LAT, H.E.S.S.
  Status: no convincing signal ...

Understanding the nature of DM besides Gravitation

Strategies of DM searches Collider experiments: SM SM $\xrightarrow{annihilate} \chi\chi$

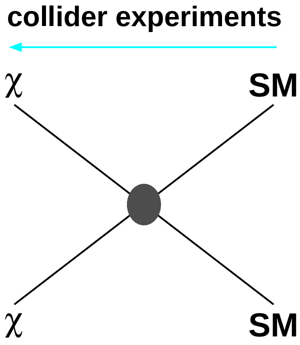

- SM SM $\xrightarrow{heavyMediator} \chi\chi$
  To measure: "missing energy".
  Experiments: ATLAS, CMS.
  Status: no signal.
  limits: $\sim (10^{-41} - 10^{-45}) cm^2$,
  channels dependent.
- SM SM $\xrightarrow{mainlyLightMediator} \chi\chi$
  To measure: other possible "hidden" sectors, like dark photon etc.
  Technology: beam hits on a fix target.
  Experiments: SHiP (https://ship.web.cern.ch/ship/), LDMX (sub-GeV, arXiv: 1808.05219)
  Status: construction or early stage of proposal.

Understanding the nature of DM besides Gravitation

Strategies of DM searches DM direct detection: scattering χ from SM particles.

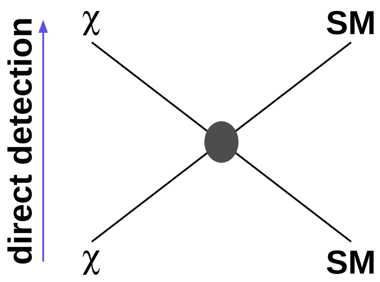

- $\chi + SM \xrightarrow{elasticScatter} \chi + SM$
  Deep underground labs, block Bkgds from cosmic rays.
  To measure: WIMP-nucleon recoils.
  Experiments: $\sim$ 50.
  Status: lowest limits: $\sim 4.0 \times 10^{-47}\ cm^2$ at $\sim$ 30GeV, XENON 1T using LXe.
  Challenge: the capability of discriminating ER (Bkg) / NR (Sig) events by separating these two bands.

Understanding the nature of DM besides Gravitation

DM direct detection is faster than the Moore’s law since 2000.

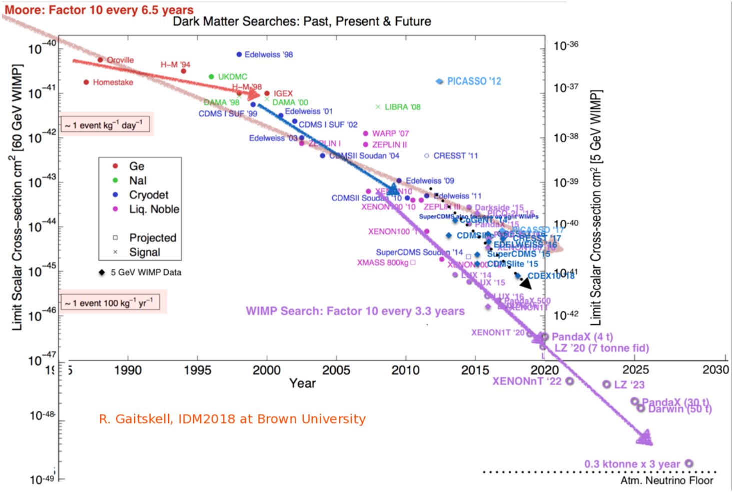

outline

BROWN

Event rate

Standard Spin Independent (S.I.) and EFT, $(\text{Kg day keV})^{-1}$

- $\frac{dE}{dR}_{SI} = \frac{\sigma_{\chi p}^{SI} A^2}{m_{red}^2(m_p)} \times N_T F_{SI}^2(E) \times \frac{\rho_\chi}{2m_\chi} \int_{v_{min}}^{\infty} \frac{f_1(v)}{v} dv$
- $\frac{\sigma_{\chi p}^{SI} A^2}{m_{red}^2(m_p)}$, particle physics.
  $\sigma_{\chi p}^{SI}$, cross-section of WIMPs and a proton; A, atomic number of target nucleus; $m_{red}(m_p)$, reduced mass of WIMPs and a nucleon.
  $N_T F_{SI}^2(E)$, nuclear physics.
  N_T, # of target nucleon per kg detector, $F_{SI}^2(E)$, form factor.
  $\frac{\rho_\chi}{2m_\chi} \int_{v_{min}}^{\infty} \frac{f_1(v)}{v} dv$, astrophysics.
  ρ_χ, observed dark matter mass density, a factor of 2 uncertainty. m_χ , mass of dark matter. v_{min}, minimum speed of WIMPs could deposit detectable energy, $f_1(v)$, local speed distribution of WIMPs.
  With the latest Gaia data, arXiv: 1807.02519 addressed a discrepancy to the Standard Halo Model. If it's correct, the local WIMP speed would be slightly smaller than typically expected. As a result, the event rate of DM direct detection will be changed.

Event rate

Standard Spin Independent (S.I.) and EFT, (Kg day keV)$^{-1}$

- $\frac{dE}{dR}_{SI} = \frac{\sigma^{SI}_{\chi p} A^2}{m^2_{red}(m_p)} \times N_T F^2_{SI}(E) \times \frac{\rho_\chi}{2m_\chi} \int_{v_{min}}^{\infty} \frac{f_1(v)}{v} dv$
- $\frac{\sigma^{SI}_{\chi p} A^2}{m^2_{red}(m_p)}$, particle physics.

  $\sigma^{SI}_{\chi p}$, cross-section of WIMPs and a proton; A, atomic number of target nucleus; $m_{red}(m_p)$, reduced mass of WIMPs and a nucleon.

  $N_T F^2_{SI}(E)$, nuclear physics.

  N_T, # of target nucleon per kg detector, $F^2_{SI}(E)$, form factor.

  $\frac{\rho_\chi}{2m_\chi} \int_{v_{min}}^{\infty} \frac{f_1(v)}{v} dv$, astrophysics.

  ρ_χ, observed dark matter mass density, a factor of 2 uncertainty. m_χ , mass of dark matter. v_{min}, minimum speed of WIMPs could deposit detectable energy, $f_1(v)$, local speed distribution of WIMPs.

  With the latest Gaia data, arXiv: 1807.02519 addressed a discrepancy to the Standard Halo Model. If it's correct, the local WIMP speed would be slightly smaller than typically expected. As a result, the event rate of DM direct detection will be changed.

Backgrounds

Reducible Backgrounds

- Backgrounds due to cosmic rays.
  Solution: Deep underground; outer detector as a veto.
- Radioactive materils.
  Solution: selecting low radioactive material (and screening)

Reject Background events

- ER background
  Key solution: S2 / S1 band for LXe; PSD for LAr; none for TES readout detectors like SuperCDMS.
- NR backgrounds (neutrons)
  Solution: veto, fiducial volume cut etc.

Model remained Backgrounds

- Modeling background to know as precisely as possible.
- Comparing background events with WIMPs search data.

outline

BROWN

Theoretical models: standard SI / SD and EFT

- Assuming heavy mediator, two main stream models: SI / SD and Effective Field Theory (EFT).
- Comparing to traditional SI/SD, EFT provides a more complete frame-work to characterize two Fermions’ elastic scattering.
- There are other possible models: light mediator, axion and axion-like-particles, ...

Event rate, standard Spin Independent (SI) and EFT, (Kg day keV)$^{-1}$

- $\frac{dE}{dR}_{SI} = N_T \cdot \frac{\rho_\chi}{2m_\chi} \cdot \frac{A^2}{m^2_{red}(m_p)} \cdot \sigma^{SI}_{\chi p} \cdot F^2_{SI}(E) \cdot \int_{v_{min}}^{\infty} \frac{f_1(v)}{v} dv$
- $\frac{dE}{dR}_{EFT} = N_T \cdot \frac{\rho_\chi}{2m_\chi} \cdot \frac{A^2}{m^2_{red}(m_p)} \cdot \mathcal{O}s \cdot \int_{v_{min}}^{\infty} \frac{f_1(v)}{v} dv$ [∼naïvely∼]
- $\mathcal{O}s$ represents the nuclear response of a detector to WIMPs.

BROWN

EFT successfully described a weak-interaction, beta decay in 1930s

The Fermi model of weak interaction is an EFT

- In the experiments of nuclear beta decay, physicists observed the energy spectrum of the electron is continuous. To interpret it, Pauli introduced the neutrino.
- Fermi proposed the Lagrangian to describe the beta decay.
- It has been widely considered as a “brilliantly successful” theory until 1960s the weak interaction theory arose.

Phenomenological model based on four-point interactions (Fermi, 1932).

$$\mathcal{L}_{\text{Fermi}} = -2\sqrt{2}G_F \left[\bar{\Psi}_d \; \gamma_\mu \frac{1-\gamma^5}{2} \; \Psi_u\right]\left[\bar{\Psi}_{\nu_e} \; \gamma^\mu \frac{1-\gamma^5}{2} \; \Psi_e\right] + \text{h.c.} \; .$$

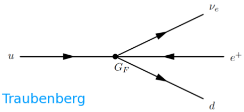

B. Fuks & M. Traubenberg

- Does this indicate we can understand DM only until 2040s ? Since 2040s - 2010s $\sim$ = 30 years = 1960s - 1930s $\ddot{\smile}$.

EFT successfully described a weak-interaction, beta decay in 1930s

The Fermi model of weak interaction is an EFT

- In the experiments of nuclear beta decay, physicists observed the energy spectrum of the electron is continuous. To interpret it, Pauli introduced the neutrino.
- Fermi proposed the Lagrangian to describe the beta decay.
- It has been widely considered as a "brilliantly successful" theory until 1960s the weak interaction theory arose.

Phenomenological model based on four-point interactions (Fermi, 1932).

$$\mathcal{L}_{\text{Fermi}} = -2\sqrt{2}G_F \left[\bar{\Psi}_d\, \gamma_\mu \frac{1-\gamma^5}{2}\, \Psi_u\right]\left[\bar{\Psi}_{\nu_e}\, \gamma^\mu \frac{1-\gamma^5}{2}\, \Psi_e\right] + \text{h.c.}\ .$$

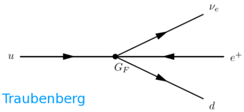

B. Fuks & M. Traubenberg

Solution: a gauge theory (Glashow, Salam, Weinberg, 60-70, [Nobel prize, 1979]).

* Four fermion interactions can be seen as a *s*-channel diagram.

* Introduction of a **new gauge boson** W_μ.

* This boson couples to fermions with a **strength** g_w.

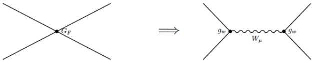

G_F $\qquad\qquad \frac{g_w^2}{p^2 - m_w^2} \approx -\frac{g_w^2}{m_w^2}$

* Prediction: $g_w \sim \mathcal{O}(1) \Rightarrow m_w \sim 100$ GeV.

B. Fuks & M. Traubenberg

- Does this indicate we can understand DM only until 2040s ? Since 2040s - 2010s $\sim$ = 30 years = 1960s - 1930s $\ddot{\smile}$.

EFT $\mathcal{O}$s

$\mathcal{O}_1 = 1_\chi 1_N$ (Standard Spin Independent)

$\mathcal{O}_3 = i\vec{S}_N \cdot \left[\frac{\vec{q}}{m_N} \times \vec{v}^\perp\right]$

$\mathcal{O}_4 = \vec{S}_\chi \cdot \vec{S}_N$ (Standard Spin Dependent)

$\mathcal{O}_5 = i\vec{S}_\chi \cdot \left[\frac{\vec{q}}{m_N} \times \vec{v}^\perp\right]$

$\mathcal{O}_6 = \left[\vec{S}_\chi \cdot \frac{\vec{q}}{m_N}\right]\left[\vec{S}_N \cdot \frac{\vec{q}}{m_N}\right]$

$\mathcal{O}_7 = \vec{S}_N \cdot \vec{v}^\perp$

$\mathcal{O}_8 = \vec{S}_\chi \cdot \vec{v}^\perp$

$\mathcal{O}_9 = i\vec{S}_\chi \cdot \left[\vec{S}_N \times \frac{\vec{q}}{m_N}\right]$

$\mathcal{O}_{10} = i\vec{S}_N \cdot \frac{\vec{q}}{m_N}$

$\mathcal{O}_{11} = i\vec{S}_\chi \cdot \frac{\vec{q}}{m_N}$

$\mathcal{O}_{12} = \vec{S}_\chi \cdot \left[\vec{S}_N \times \vec{v}^\perp\right]$

$\mathcal{O}_{13} = i\left[\vec{S}_\chi \cdot \vec{v}^\perp\right]\left[\vec{S}_N \cdot \frac{\vec{q}}{m_N}\right]$

$\mathcal{O}_{14} = i\left[\vec{S}_\chi \cdot \frac{\vec{q}}{m_N}\right]\left[\vec{S}_N \cdot \vec{v}^\perp\right]$

$\mathcal{O}_{15} = -\left[\vec{S}_\chi \cdot \frac{\vec{q}}{m_N}\right]\left[\left(\vec{S}_N \times \vec{v}^\perp\right) \cdot \frac{\vec{q}}{m_N}\right]$

$\mathcal{O}_{u}$ <=> S.I.

Others <=> S.D.

Arxiv : 1308.6288

ArxiV : 1008.1591

Arxiv : 1203.3542

ArxiV : 1503.03379

- The first paper listed all of the $\mathcal{O}_s$ for F-F interactions. (JHEP11(2006) 005).
- The first paper applying "JHEP11(2006) 005" into DM, arXiv: 1308.6288.
- Galilean-invariant (NR). Elastic scattering.
- Four parameters:
  DM velocity, $\vec{v} \sim 10^{-3}c$;
  momentum transfer, $\vec{q}$;
  DM spin, $\vec{S}_\chi$;
  nucleon spin; $\vec{S}_N$.
- $\mathcal{O}_1$ and $\mathcal{O}_4$, tree level;
  $\mathcal{O}_1$ = standard S.I. ; $\mathcal{O}_4$ = standard S.D.
  others $\mathcal{O}_s$, LO, NLO, N^{2}LO, N^{3}LO.
- The Fermi interpretation on the weak interaction in 1930s is one of the most famous examples of EFT (previous slide.).

The key difference between EFT and standard SI / SD (naïvely)

Whether or not considered the transferred momentum of a DM-detector scattering

- Left picture: a long wavelength corresponds to a small momentum transferred scattering; EFT and Standard SI/SD is the same for this kind of scattering.
- Right picture: a short wavelength corresponds to big momentum transferred scattering; standard SI/SD uses a form factor to characterize the “reduced” recoil energy to the hit nuclei while ignore the interactions caused by the transferred momentum; EFT fully characterizes all of possible interactions with operators.

The key difference between EFT and standard SI / SD

- Left picture: the interactions between DM and detector by considering the transferred momentum under EFT.
- Right picture: as a result, by considering the “extra” interactions caused by EFT operators, the recoil energy of EFT operators are higher than standard SI/SD.

The point-nucleus world is what we thought we could probe
But the derivative coupling world is is easy to see, with the right target

$$
\begin{aligned}
R_M^{\tau\tau'}(\vec{v}_T^{\perp 2}, \frac{\vec{q}^2}{m_N^2}) &= c_1^\tau c_1^{\tau'} + \frac{j_\chi(j_\chi+1)}{3}\left[\frac{\vec{q}^2}{m_N^2}\vec{v}_T^{\perp 2} c_5^\tau c_5^{\tau'} + \vec{v}_T^{\perp 2} c_8^\tau c_8^{\tau'} + \frac{\vec{q}^2}{m_N^2} c_{11}^\tau c_{11}^{\tau'}\right] \\
R_{\Phi''}^{\tau\tau'}(\vec{v}_T^{\perp 2}, \frac{\vec{q}^2}{m_N^2}) &= \frac{\vec{q}^2}{4m_N^2} c_3^\tau c_3^{\tau'} + \frac{j_\chi(j_\chi+1)}{12}\left(c_{12}^\tau - \frac{\vec{q}^2}{m_N^2} c_{15}^\tau\right)\left(c_{12}^{\tau'} - \frac{\vec{q}^2}{m_N^2} c_{15}^{\tau'}\right) \\
R_{\Phi'' M}^{\tau\tau'}(\vec{v}_T^{\perp 2}, \frac{\vec{q}^2}{m_N^2}) &= c_3^\tau c_1^{\tau'} + \frac{j_\chi(j_\chi+1)}{3}\left(c_{12}^\tau - \frac{\vec{q}^2}{m_N^2} c_{15}^\tau\right) c_{11}^{\tau'} \\
R_{\tilde{\Phi}'}^{\tau\tau'}(\vec{v}_T^{\perp 2}, \frac{\vec{q}^2}{m_N^2}) &= \frac{j_\chi(j_\chi+1)}{12}\left[c_{12}^\tau c_{12}^{\tau'} + \frac{\vec{q}^2}{m_N^2} c_{13}^\tau c_{13}^{\tau'}\right] \\
R_{\Sigma''}^{\tau\tau'}(\vec{v}_T^{\perp 2}, \frac{\vec{q}^2}{m_N^2}) &= \frac{\vec{q}^2}{4m_N^2} c_{10}^\tau c_{10}^{\tau'} + \frac{j_\chi(j_\chi+1)}{12}\left[c_4^\tau c_4^{\tau'} + \right. \\
&\left. \frac{\vec{q}^2}{m_N^2}(c_4^\tau c_6^{\tau'} + c_6^\tau c_4^{\tau'}) + \frac{\vec{q}^4}{m_N^4} c_6^\tau c_6^{\tau'} + \vec{v}_T^{\perp 2} c_{12}^\tau c_{12}^{\tau'} + \frac{\vec{q}^2}{m_N^2}\vec{v}_T^{\perp 2} c_{13}^\tau c_{13}^{\tau'}\right] \\
R_{\Sigma'}^{\tau\tau'}(\vec{v}_T^{\perp 2}, \frac{\vec{q}^2}{m_N^2}) &= \frac{1}{8}\left[\frac{\vec{q}^2}{m_N^2}\vec{v}_T^{\perp 2} c_3^\tau c_3^{\tau'} + \vec{v}_T^{\perp 2} c_7^\tau c_7^{\tau'}\right] + \frac{j_\chi(j_\chi+1)}{12}\left[c_4^\tau c_4^{\tau'} + \right. \\
&\left. \frac{\vec{q}^2}{m_N^2} c_9^\tau c_9^{\tau'} + \frac{\vec{v}_T^{\perp 2}}{2}\left(c_{12}^\tau - \frac{\vec{q}^2}{m_N^2} c_{15}^\tau\right)\left(c_{12}^{\tau'} - \frac{\vec{q}^2}{m_N^2} c_{15}^{\tau'}\right) + \frac{\vec{q}^2}{2m_N^2}\vec{v}_T^{\perp 2} c_{14}^\tau c_{14}^{\tau'}\right] \\
R_{\Delta}^{\tau\tau'}(\vec{v}_T^{\perp 2}, \frac{\vec{q}^2}{m_N^2}) &= \frac{j_\chi(j_\chi+1)}{3}\left[\frac{\vec{q}^2}{m_N^2} c_5^\tau c_5^{\tau'} + c_8^\tau c_8^{\tau'}\right] \\
R_{\Delta\Sigma'}^{\tau\tau'}(\vec{v}_T^{\perp 2}, \frac{\vec{q}^2}{m_N^2}) &= \frac{j_\chi(j_\chi+1)}{3}\left[c_5^\tau c_4^{\tau'} - c_8^\tau c_9^{\tau'}\right].
\end{aligned}
$$

W. Haxton

TABLE I. The upper energy threshold E_{max} (in keV_{nr}) for each of the effective field theory operators, such that an energy window from 0 to E_{max} captures either 50% or 90% of WIMP-neutron recoil events for the given operator and WIMP mass.

Nicole Larson's EFT draft paper

Operator	50-GeV WIMP $E_{max}^{50\%}$ (keV_{nr})	50-GeV WIMP $E_{max}^{90\%}$ (keV_{nr})	500-GeV WIMP $E_{max}^{50\%}$ (keV_{nr})	500-GeV WIMP $E_{max}^{90\%}$ (keV_{nr})
SI	10.8	27.3	16.6	44.7
$\mathcal{O}_1$	6.8	21.7	11.8	43.8
$\mathcal{O}_3$	26.4	49.1	148.1	344.4
SD	8.6	21.6	11.9	37.5
$\mathcal{O}_4$	7.0	24.0	32.8	299.6
$\mathcal{O}_5$	16.2	38.6	65.5	328.9
$\mathcal{O}_6$	33.6	64.0	267.3	433.7
$\mathcal{O}_7$	5.0	16.2	25.2	279.9
$\mathcal{O}_8$	6.8	22.2	14.5	64.8
$\mathcal{O}_9$	13.7	37.2	276.7	464.7
$\mathcal{O}_{10}$	21.7	48.6	112.6	340.4
$\mathcal{O}_{11}$	15.5	34.4	39.0	279.9
$\mathcal{O}_{12}$	17.4	38.1	34.8	176.5
$\mathcal{O}_{13}$	28.2	53.2	54.5	219.7
$\mathcal{O}_{14}$	11.9	27.9	240.9	400.0
$\mathcal{O}_{15}$	34.3	59.1	261.2	433.7

The EFT interactions in the space of particle physics (relativistic)

N. Anard etc, arXiv: 1308.6288

j	$\mathcal{L}^j_{\text{int}}$	Nonrelativistic reduction	$\sum_i c_i \mathcal{O}_i$	P/T
1	$\bar\chi\chi\bar N N$	$1_\chi 1_N$	$\mathcal{O}_1$	E/E
2	$i\bar\chi\chi\bar N\gamma^5 N$	$i\frac{\vec q}{m_N}\cdot\vec S_N$	$\mathcal{O}_{10}$	O/O
3	$i\bar\chi\gamma^5\chi\bar N N$	$-i\frac{\vec q}{m_\chi}\cdot\vec S_\chi$	$-\frac{m_N}{m_\chi}\mathcal{O}_{11}$	O/O
4	$\bar\chi\gamma^5\chi\bar N\gamma^5 N$	$-\frac{\vec q}{m_\chi}\cdot\vec S_\chi\frac{\vec q}{m_N}\cdot\vec S_N$	$-\frac{m_N}{m_\chi}\mathcal{O}_6$	E/E
5	$\bar\chi\gamma^\mu\chi\bar N\gamma_\mu N$	$1_\chi 1_N$	$\mathcal{O}_1$	E/E
6	$\bar\chi\gamma^\mu\chi\bar N i\sigma_{\mu\alpha}\frac{q^\alpha}{m_M}N$	$\frac{\vec q^{\,2}}{2m_N m_M}1_\chi 1_N + 2(\frac{\vec q}{m_\chi}\times\vec S_\chi + i\vec v^\perp)\cdot(\frac{\vec q}{m_M}\times\vec S_N)$	$\frac{\vec q^{\,2}}{2m_N m_M}\mathcal{O}_1 - 2\frac{m_N}{m_M}\mathcal{O}_3 + 2\frac{m_N^2}{m_M m_\chi}(\frac{q^2}{m_N^2}\mathcal{O}_4 - \mathcal{O}_6)$	E/E
7	$\bar\chi\gamma^\mu\chi\bar N\gamma_\mu\gamma^5 N$	$-2\vec S_N\cdot\vec v^\perp + \frac{2}{m_\chi}i\vec S_\chi\cdot(\vec S_N\times\vec q)$	$-2\mathcal{O}_7 + 2\frac{m_N}{m_\chi}\mathcal{O}_9$	O/E
8	$i\bar\chi\gamma^\mu\chi\bar N i\sigma_{\mu\alpha}\frac{q^\alpha}{m_M}\gamma^5 N$	$2i\frac{\vec q}{m_M}\cdot\vec S_N$	$2\frac{m_N}{m_M}\mathcal{O}_{10}$	O/O
9	$\bar\chi i\sigma^{\mu\nu}\frac{q_\nu}{m_M}\chi\bar N\gamma_\mu N$	$-\frac{\vec q^{\,2}}{2m_\chi m_M}1_\chi 1_N - 2(\frac{\vec q}{m_N}\times\vec S_N + i\vec v^\perp)\cdot(\frac{\vec q}{m_M}\times\vec S_\chi)$	$-\frac{\vec q^{\,2}}{2m_\chi m_M}\mathcal{O}_1 + \frac{2m_N}{m_M}\mathcal{O}_5 - 2\frac{m_N}{m_M}(\frac{\vec q^{\,2}}{m_N^2}\mathcal{O}_4 - \mathcal{O}_6)$	E/E
10	$\bar\chi i\sigma^{\mu\nu}\frac{q_\nu}{m_M}\chi\bar N i\sigma_{\mu\alpha}\frac{q^\alpha}{m_M}N$	$4(\frac{\vec q}{m_M}\times\vec S_\chi)\cdot(\frac{\vec q}{m_M}\times\vec S_N)$	$4(\frac{\vec q^{\,2}}{m_M^2}\mathcal{O}_4 - \frac{m_N^2}{m_M^2}\mathcal{O}_6)$	E/E
11	$\bar\chi i\sigma^{\mu\nu}\frac{q_\nu}{m_M}\chi\bar N\gamma^\mu\gamma^5 N$	$4i(\frac{\vec q}{m_M}\times\vec S_\chi)\cdot\vec S_N$	$4\frac{m_N}{m_M}\mathcal{O}_9$	O/E
12	$i\bar\chi i\sigma^{\mu\nu}\frac{q_\nu}{m_M}\chi\bar N i\sigma_{\mu\alpha}\frac{q^\alpha}{m_M}\gamma^5 N$	$-[i\frac{\vec q^{\,2}}{m_\chi m_M} - 4\vec v^\perp\cdot(\frac{\vec q}{m_M}\times\vec S_\chi)]\frac{\vec q}{m_M}\cdot\vec S_N$	$-\frac{m_N}{m_\chi}\frac{\vec q^{\,2}}{m_M^2}\mathcal{O}_{10} - 4\frac{\vec q^{\,2}}{m_M^2}\mathcal{O}_{12} - 4\frac{m_N^2}{m_M^2}\mathcal{O}_{15}$	O/O
13	$\bar\chi\gamma^\mu\gamma^5\chi\bar N\gamma_\mu N$	$2\vec v^\perp\cdot\vec S_\chi + 2i\vec S_\chi\cdot(\vec S_N\times\frac{\vec q}{m_N})$	$2\mathcal{O}_8 + 2\mathcal{O}_9$	O/E
14	$\bar\chi\gamma^\mu\gamma^5\chi\bar N i\sigma_{\mu\alpha}\frac{q^\alpha}{m_M}N$	$4i\vec S_\chi\cdot(\frac{\vec q}{m_M}\times\vec S_N)$	$-4\frac{m_N}{m_M}\mathcal{O}_9$	O/E
15	$\bar\chi\gamma^\mu\gamma^5\chi\bar N\gamma^\mu\gamma^5 N$	$-4\vec S_\chi\cdot\vec S_N$	$-4\mathcal{O}_4$	E/E
16	$i\bar\chi\gamma^\mu\gamma^5\chi\bar N i\sigma_{\mu\alpha}\frac{q^\alpha}{m_M}\gamma^5 N$	$4i\vec v^\perp\cdot\vec S_\chi\frac{\vec q}{m_M}\cdot\vec S_N$	$4\frac{m_N}{m_M}\mathcal{O}_{13}$	E/O
17	$i\bar\chi i\sigma^{\mu\nu}\frac{q_\nu}{m_M}\gamma^5\chi\bar N\gamma_\mu N$	$2i\frac{\vec q}{m_M}\cdot\vec S_\chi$	$2\frac{m_N}{m_M}\mathcal{O}_{11}$	O/O
18	$i\bar\chi i\sigma^{\mu\nu}\frac{q_\nu}{m_M}\gamma^5\chi\bar N i\sigma_{\mu\alpha}\frac{q^\alpha}{m_M}N$	$\frac{\vec q}{m_M}\cdot\vec S_\chi[i\frac{\vec q^{\,2}}{m_N m_M} - 4\vec v^\perp\cdot(\frac{\vec q}{m_M}\times\vec S_N)]$	$\frac{\vec q^{\,2}}{m_M^2}\mathcal{O}_{11} + 4\frac{m_N^2}{m_M^2}\mathcal{O}_{15}$	O/O
19	$i\bar\chi i\sigma^{\mu\nu}\frac{q_\nu}{m_M}\gamma^5\chi\bar N\gamma_\mu\gamma^5 N$	$-4i\frac{\vec q}{m_M}\cdot\vec S_\chi\vec v_\perp\cdot\vec S_N$	$-4\frac{m_N}{m_M}\mathcal{O}_{14}$	E/O
20	$i\bar\chi i\sigma^{\mu\nu}\frac{q_\nu}{m_M}\gamma^5\chi\bar N i\sigma_{\mu\alpha}\frac{q^\alpha}{m_M}\gamma^5 N$	$4\frac{\vec q}{m_M}\cdot\vec S_\chi\frac{\vec q}{m_M}\cdot\vec S_N$	$4\frac{m_N^2}{m_M^2}\mathcal{O}_6$	E/E

BROWN

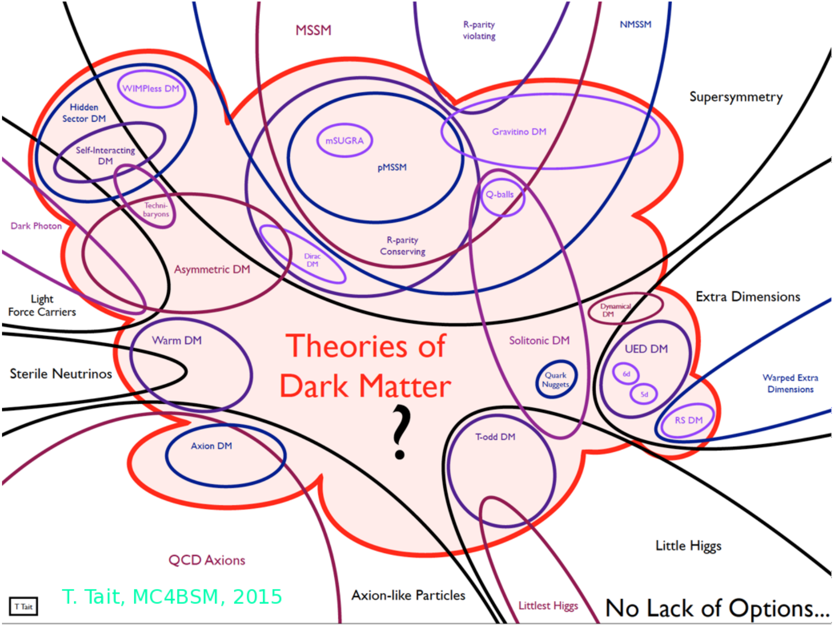
MSSM
R-parity
violating
NMSSM
Supersymmetry
WIMPless DM
Hidden
Sector DM
Self-Interacting
DM
Techni-
baryons
mSUGRA
pMSSM
Gravitino DM
Q-balls
Dark Photon
Dirac
DM
R-parity
Conserving
Asymmetric DM
Light
Force Carriers
Extra Dimensions
Dynamical
DM
Warm DM
Theories of
Dark Matter
?
Solitonic DM
UED DM
6d
5d
Quark
Nuggets
Warped Extra
Dimensions
RS DM
Sterile Neutrinos
Axion DM
T-odd DM
Little Higgs
QCD Axions
T Tait
T. Tait, MC4BSM, 2015
Axion-like Particles
Littlest Higgs
No Lack of Options...

outline

The progress of DM direct detection, by Sep 2017

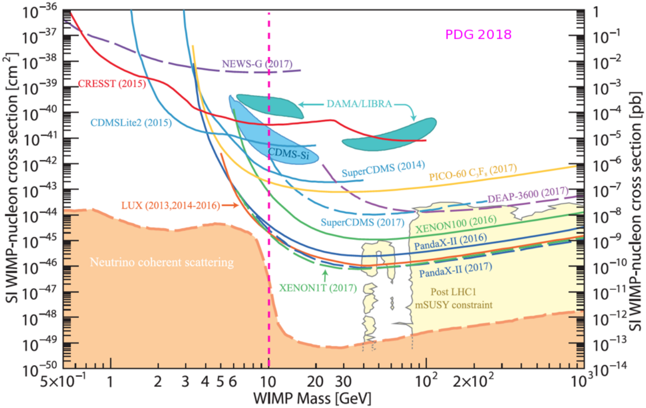

- CDMS-Si, CoGeNT and DAMA/LIBRA claimed observations have been excluded.
- High mass ($\sim$ 10 - 1000 GeV/c^2) searches : DarkSide, DEAP, LUX, PandaX, XENON and XMASS etc.
  LXe, S2 / S1 band for ER, NR .

  LAr TPC, PSD
- Low mass ($\sim$ 1 - 10 GeV/c^2) : CDEX, (Super)CDMS, CRESST, DAMIC, EDELWEISS, PICO and SIMPLE etc.

  Heat and / or ionization.

outline

Dark Matter In CCDs (DAMIC) science

- Left plot : Region Of Interest(ROI) : low mass WIMP ($\sim$ 1 - 10 GeV / c^2), complementary to high-mass noble liquid detectors.
- Right plot : DAMIC collaboration (not the latest).

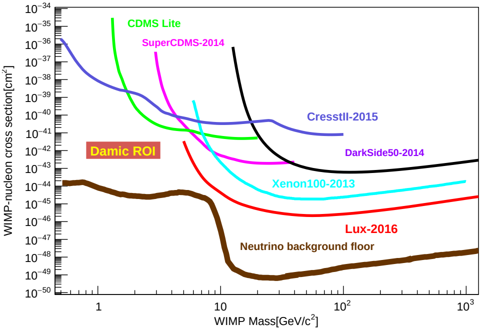

Two universities from the US, one National Laboratory and 6 institutions from abroad.

Centro Atomico Bariloche, Argentina
Fermi National Accelerator Laboratory, USA
SNOLAB, Canada
Universidad Federal Rio Janeiro, Brazil
Universidad Nacional de Asuncion, Paraguay
Universidad Nacional Autonoma de Mexico
University of Chicago , USA
University of Michigan, USA
University of Zurich, Switzerland

BROWN

DAMIC CCDs

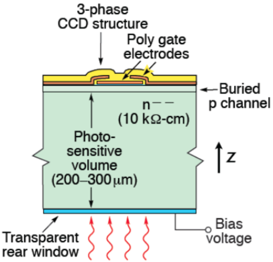
3-phase
CCD structure
Poly gate
electrodes
Buried
p channel
n^{--}
(10 kΩ-cm)
Photo-
sensitive
volume
(200–300 μm)
z
Transparent
rear window
Bias
voltage

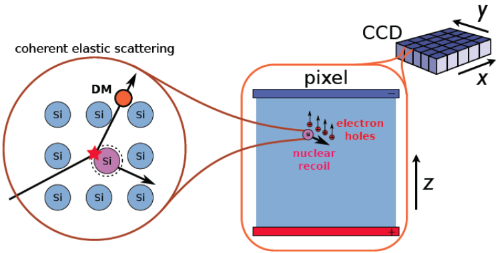
coherent elastic scattering
DM
Si
CCD
y
x
pixel
electron
holes
nuclear
recoil
z

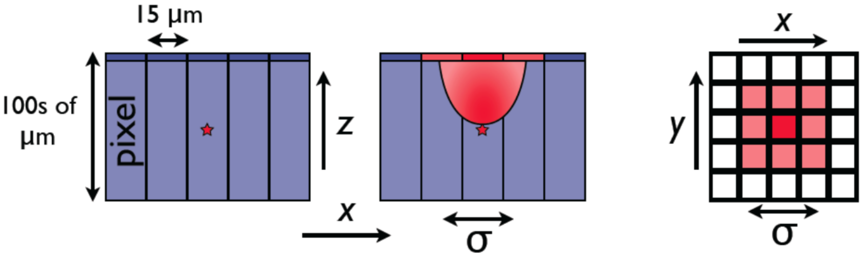
15 μm
100s of
μm
pixel
z
x
σ
x
y
σ

CCD charge readout

- Charge reading in controlled sequences. Deposited charge in each pixel can be reconstructed offline.

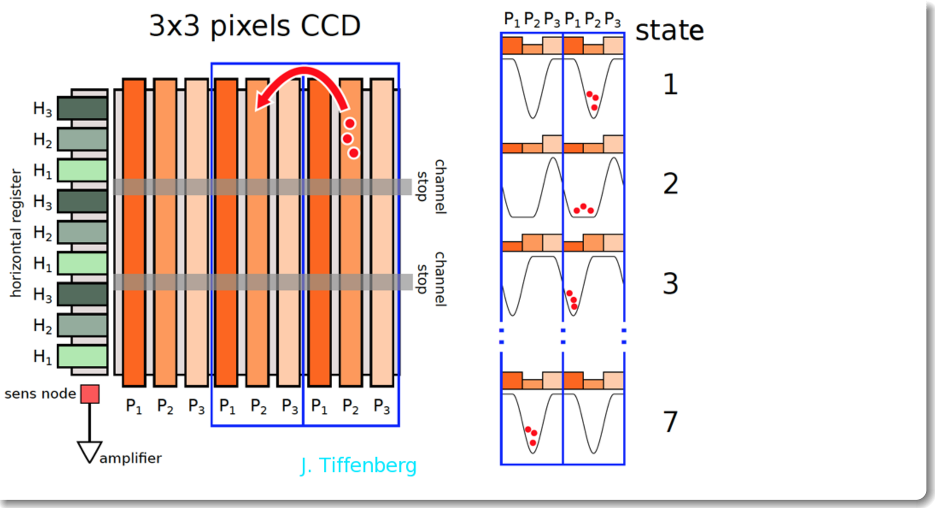

signals measured by a DAMIC CCD

- Image of a 2k×4k CCDs (Top view). A cell indicates (naively) a pixel.

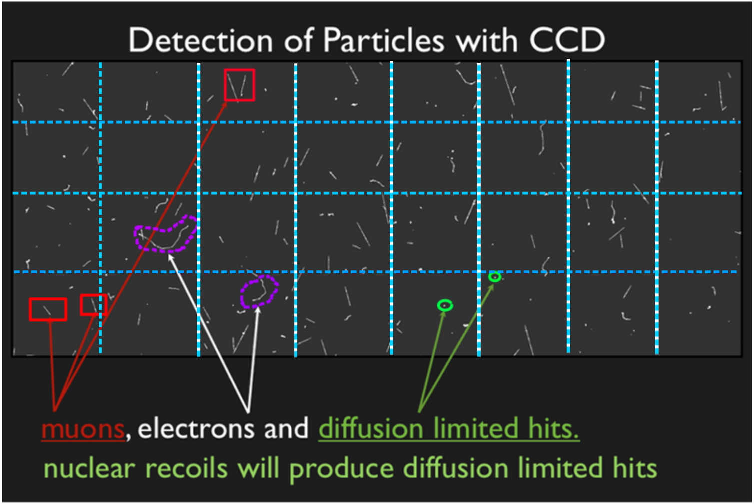

signals measured by a DAMIC CCD

- Image of a 2k$\times$4k CCDs (Top view).

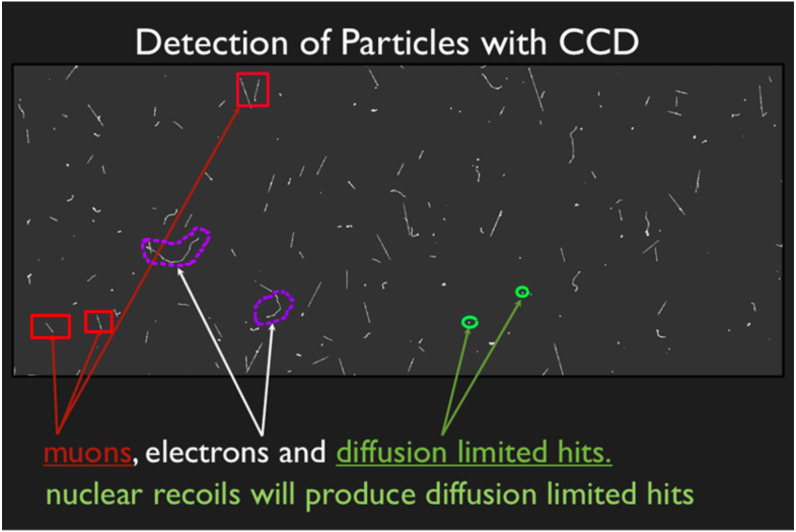

CCDs low noise ⇒ good for low mass WIMP hunting

- Left plot : 1.8 e^- noise(RMS) ⇒ 5σ noise ≊ 40 eV.
- Right plot: Red curve : event rates, 5 GeV WIMPs, Si detector, S.I..
  pink curve : event rates, 35 GeV WIMPs, Si detector, S.I..
  aqua line : E_R = 240 eV, translate from 5σ noise of CCDs, 40 eV.
  blue broken line : E_R = 3.0 keV, CDMS Si detector.

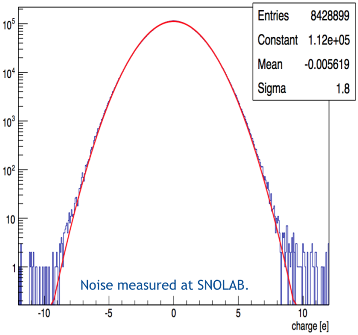

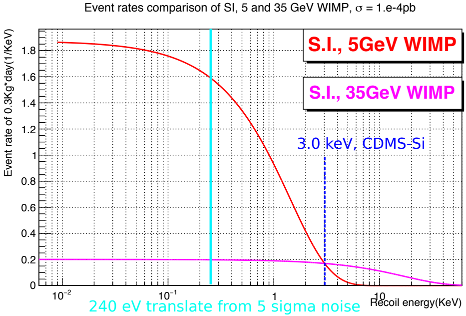

DAMIC-100 in Snolab

- DAMIC-100 CCDs: high-resistivity, 675 μm, 16 M Pix, 5.6 g per piece. Developed by LBNL Microsystems Lab. 18 CCDs: $18 \times 5.6g = 100.8g$.
- Commission since April, 2016 (data analysis now).
- Snolab, world's second-deepest underground lab, 6010 MWE shielding.

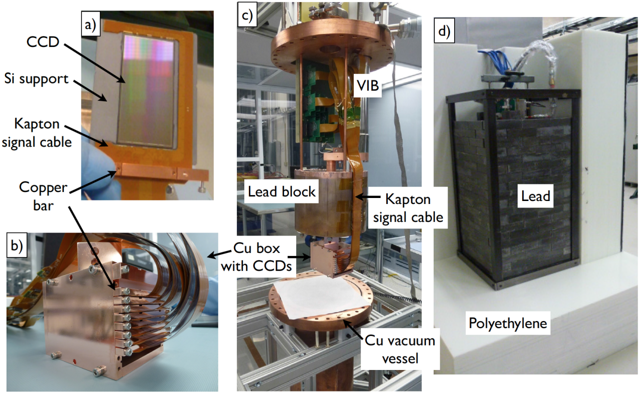

Background study

- Left plot : In 2015, quite a few configurations to understand bkdgs.
- Right plot : 5 dru ((keV kg day)$^{-1}$) has been reached, close to our goal : 1 *dru*.

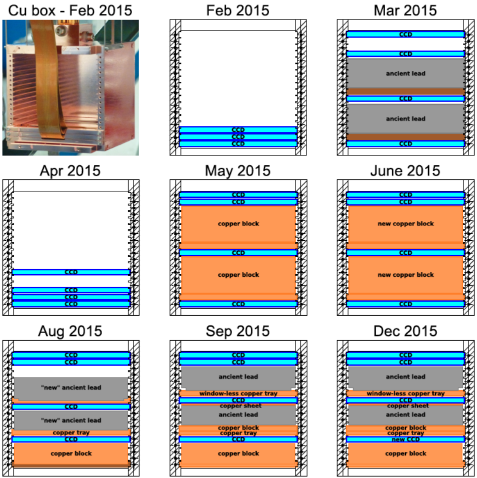

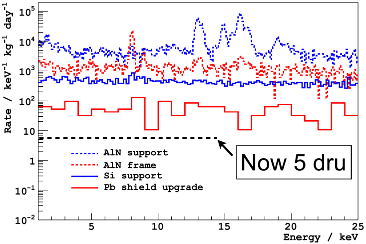

outline

BROWN

DAMIC CCDs: energy response

CCD energy calibrations with variant X-rays

- Left: energy response linearity: 300 eV - 30 keV.
- Right: energy measured with fluorescence X-rays.

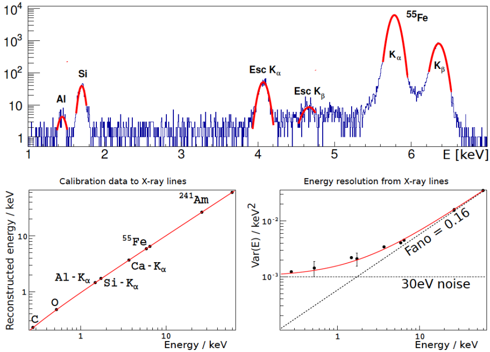

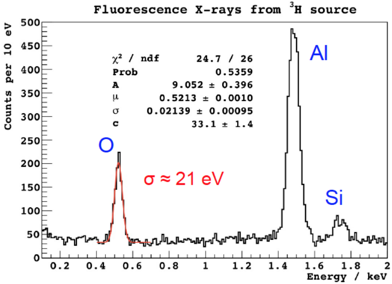

Quenching Factor (QF) measurement for Si at low E_R: QF = E_i / E_r

- An incoming WIMP deposits energy, E_r, in the detector. Part of the E_r can be measured by a CCD, E_i.
- Can't find a WIMPs source to calibrate our CCDs ☹
- Fast neutrons scatter a detector same as WIMPs ⇒ calibrate the detector with fast neutrons.

- Lindhard, a classic model for QF.
- For silicon, QF for $E_R > 4$ keV, measured.
- DAMIC has launched two tests on QF:
  1. E_R :$\sim$ 1.5 KeV - 20.0 KeV.
  2. E_R :$\sim$ 0.6 KeV - 2.0 KeV.

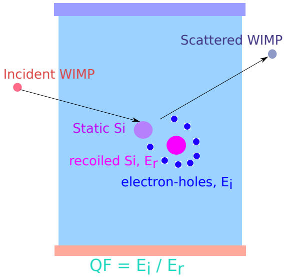

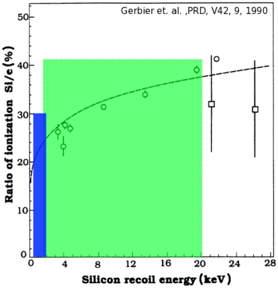

QF Beam Test (BT)

- Left plot : schematic drawing; right plot : a picture of BT.
- E_i measured by the SDD directly.
- With kinematics, one can figure out $E_r = E_{NR} = f(\Delta t, \theta)$.
- Beam test at University of Notre Dame, IN, USA (Thanks.).
- SDD (E_i), neutron beam and scintillator bars (E_r) were calibrated before BT.

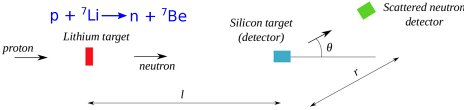

$$E_{NR} = E_n \frac{2}{(A+1)^2}\left[A + \sin^2\theta - \cos\theta\sqrt{A^2 - \sin^2\theta}\right]$$

$$E_n = \frac{m}{2(\Delta t)^2}\left[l + r\frac{(A+1)}{\cos\theta + \sqrt{A^2 - \sin^2\theta}}\right]^2$$

- θ Scattering angle
- A Atomic mass
- E_n Neutron energy
- E_{NR} Energy of Nuclear recoil
- Δt = neutron total Time-of-flight

Proton beam : 2.3MeV

Neutrons peaked at ∼550KeV among [50,600]KeV

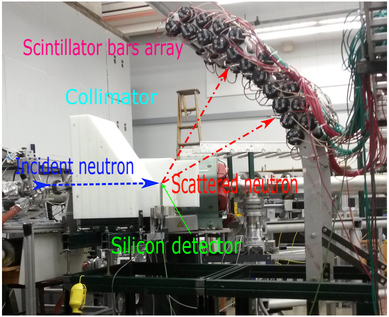

Characterize Silicon Drift Detector (SDD) for E_i

- SDD calibration (for E_i) with ^{55}Fe in Fermilab.

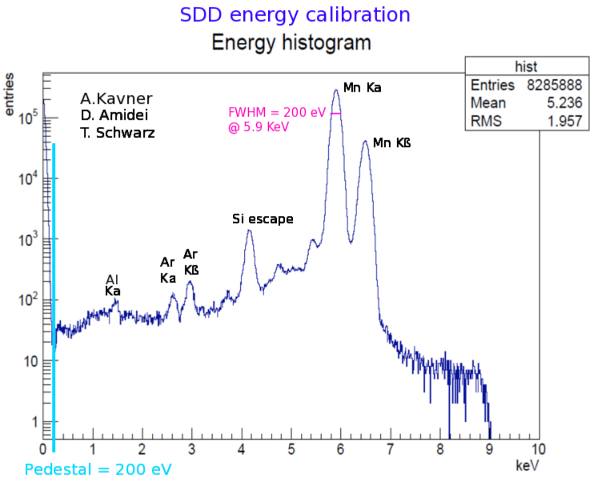

Characterization on neutron beams (for E_r)

- Left plot : Geant4 simulation.
- Right plot : Characterize neutron beam @ Notre Dame. Dots : data, histogram : Geant4 simulation.

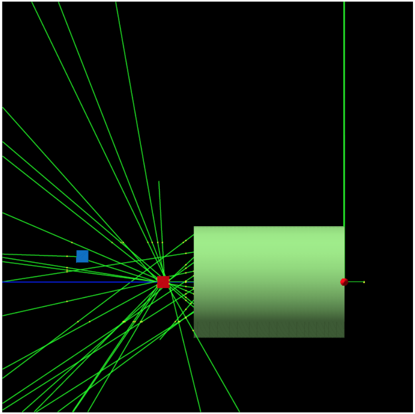

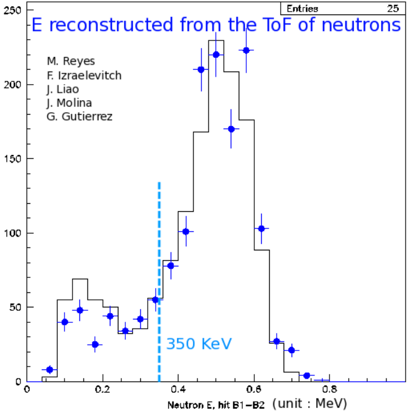

Characterize a scintillator bar (for E_r) in lab

- Plastic scintillator, EJ-200, $2.5 \times 2.5 \times 25.0\ cm^3$. Light output : 64 % Anthracene. Wavelength of Max. emission : 425 nm $\Rightarrow$ fits PMTs well, ET9954B (retired from CDF, Tevatron) .
  Density of Hydrogen / Carbon = 1.1 $\Rightarrow$ good for fast neutron detection.
  Fast rise time (0.9 ns) + long optical attenuation $\Rightarrow$ good for Time of Flight.
- Left plot : charge calibration, N_{phe} = 1.5 phe; fit : Gaussian $\otimes$ Poisson.
  Right plot : timing calibration, σ_T of $T_1 - T_2 \approxeq 2.0$ ns; fit : Gaussian.

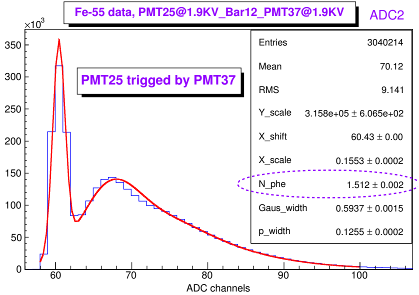

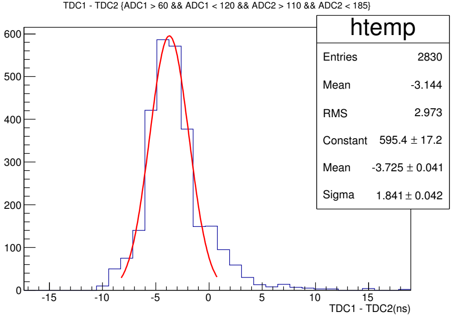

Geant 4 simulation and data comparison

- Right plot : Setup shown in Geant4 simulation.
- Lower plot: Comparison of (experimental) data and simulation.
- E_i measured by the SDD, E_r reconstructed from the ToF of scattered neutrons.

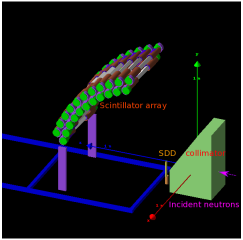

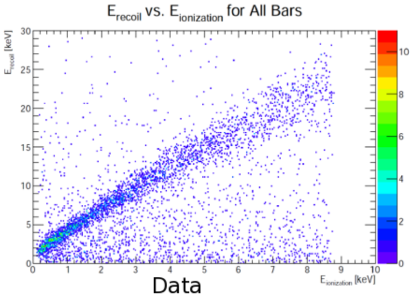

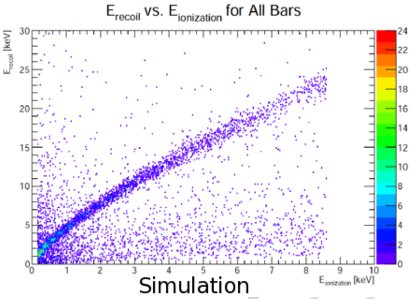

Measured QF

- Results of the QF for E_R of [1.5, 20] keV. Discrepancy to the Lindhard model exists for E_R $\sim$ 1.5 - 5.0 keV.
- For details: 2017 JINST 12 P06014.

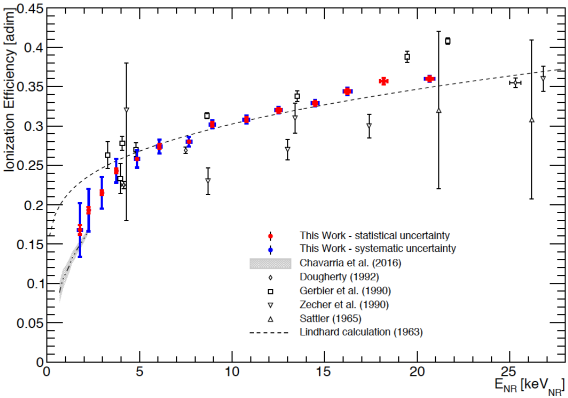

outline

BROWN

Events selection with ΔLL

- Left plot : CCD noise
- Right plot : CCD noise + signals
- We used a log-likelihood distribution, ΔLL, to select signal candidates from noise.

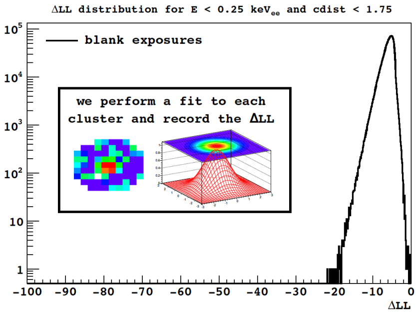

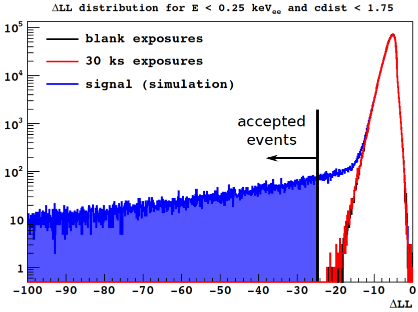

Surface events selection and detection efficiency

- Left plot : Fiducial selection of signal events.
- Right plot : detection efficiency.

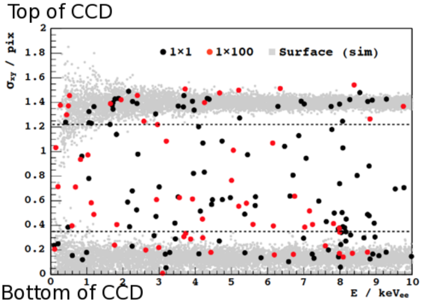

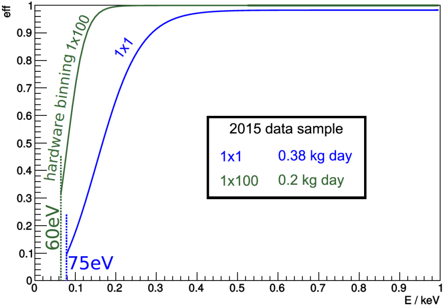

Upper limit, 90% C.L., 0.6 Kg*day, standard S.I.

PRD 94, 0282006 (2016), arXiv:1607.07410.

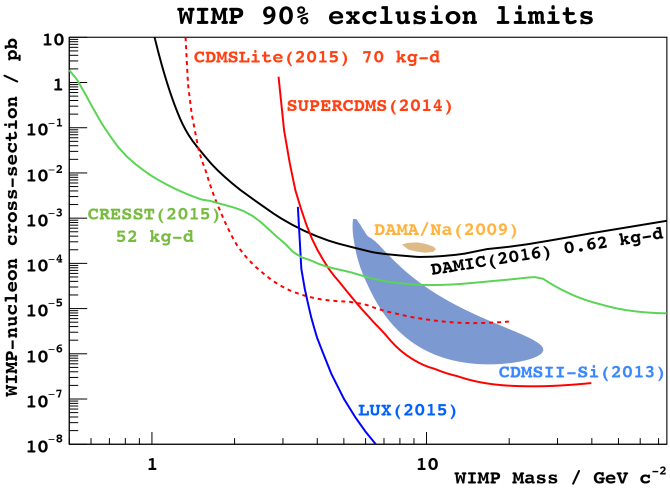

Low noise CCDs are suited for Effective Field Theory (EFT) analysis

- Event rates of all S.I. EFT $\mathcal{O}_1$ and $\mathcal{O}_5$, 5 GeV WIMPs, silicon detector.
- Cyan vertical lines: 5σ noise of DAMIC CCDs + Lindhard QF; Green: 5σ noise of DAMIC CCDs + DAMIC measured QF.
- Other two S.I. $\mathcal{O}$s: $\mathcal{O}_8$ and $\mathcal{O}_{11}$ have similar features.

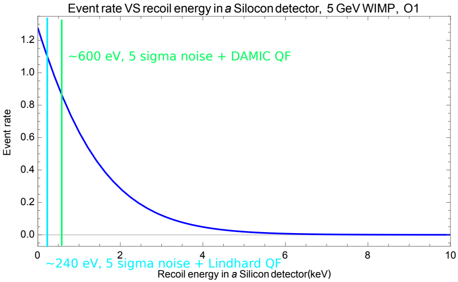

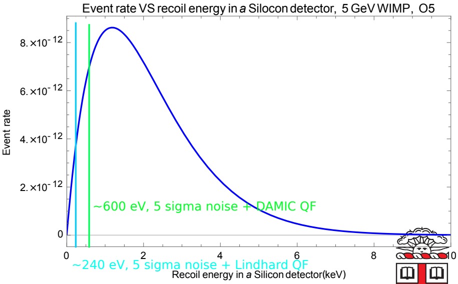

BROWN

90% C.L. upper limits, all EFT S.I. $\mathcal{O}$s and standard S.I.

- 0.6 kg*day data, QF measured by DAMIC.
- $\mathcal{O}_{11} = i\vec{S}_\chi \cdot \frac{\vec{q}}{m_N}$, is the most sensitive operator.

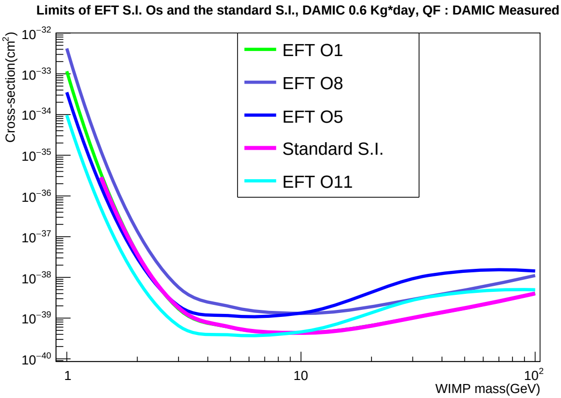

90% C.L. upper limits of all EFT S.D. $\mathcal{O}s$

- 0.6 $\times$ 5% = 0.028 kg*day data of Si-29, QF measured by DAMIC. $\mathcal{O}_{15} = -\left(\vec{S}_\chi \cdot \frac{\vec{q}}{m_N}\right)\left[\left(\vec{S}_N \times \vec{v}^\perp\right) \cdot \frac{\vec{q}}{m_N}\right]$ is the most sensitive one.

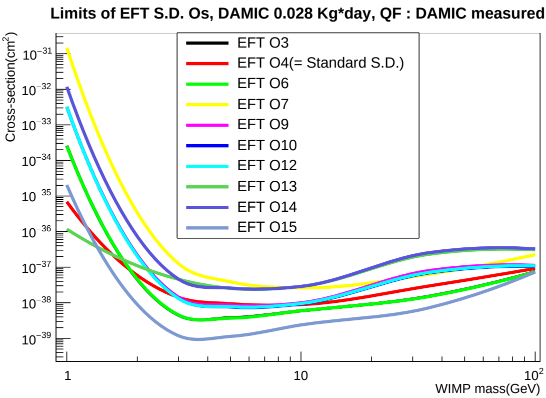

outline

BROWN

Summary for DAMIC

- DAMIC CCDs have very low noise which is good for low mass WIMIP hunting. DAMIC has measured the quenching factor of silicon down to 100s keV recoil energy. A discrepancy comparing to the Lindhard model has been observed.
- All EFT $\mathcal{O}s$ have been studied and analyzed with DAMIC $\sim$ 0.6 kg*day data. No signal has been observed. 90% C.L. upper limits with have been set.
- We find the most sensitive EFT operators of WIMP-nuclear interaction, $\mathcal{O}_{11}$ for S.I. and $\mathcal{O}_{15}$ for S.D..
- Publication 1: WIMPs search, PRD 94, 0282006 (2016), arXiv:1607.07410 .
- Publication 2 : QF calibration for Silicon, 2017 JINST 12 P06014.

Summary for DAMIC

- DAMIC CCDs have very low noise which is good for low mass WIMIP hunting. DAMIC has measured the quenching factor of silicon down to 100s keV recoil energy. A discrepancy comparing to the Lindhard model has been observed.
- All EFT $\mathcal{O}s$ have been studied and analyzed with DAMIC $\sim$ 0.6 kg*day data. No signal has been observed. 90% C.L. upper limits with have been set.
- We find the most sensitive EFT operators of WIMP-nuclear interaction, $\mathcal{O}_{11}$ for S.I. and $\mathcal{O}_{15}$ for S.D..
- Publication 1: WIMPs search, PRD 94, 0282006 (2016), arXiv:1607.07410 .
- Publication 2 : QF calibration for Silicon, 2017 JINST 12 P06014.

BROWN

Summary for DAMIC

- DAMIC CCDs have very low noise which is good for low mass WIMIP hunting. DAMIC has measured the quenching factor of silicon down to 100s keV recoil energy. A discrepancy comparing to the Lindhard model has been observed.
- All EFT $\mathcal{O}s$ have been studied and analyzed with DAMIC $\sim$ 0.6 kg*day data. No signal has been observed. 90% C.L. upper limits with have been set.
- We find the most sensitive EFT operators of WIMP-nuclear interaction, $\mathcal{O}_{11}$ for S.I. and $\mathcal{O}_{15}$ for S.D..
- Publication 1: WIMPs search, PRD 94, 0282006 (2016), arXiv:1607.07410 .
- Publication 2 : QF calibration for Silicon, 2017 JINST 12 P06014.

BROWN

Summary for DAMIC

- DAMIC CCDs have very low noise which is good for low mass WIMIP hunting. DAMIC has measured the quenching factor of silicon down to 100s keV recoil energy. A discrepancy comparing to the Lindhard model has been observed.
- All EFT $\mathcal{O}s$ have been studied and analyzed with DAMIC $\sim$ 0.6 kg*day data. No signal has been observed. 90% C.L. upper limits with have been set.
- We find the most sensitive EFT operators of WIMP-nuclear interaction, $\mathcal{O}_{11}$ for S.I. and $\mathcal{O}_{15}$ for S.D..
- Publication 1: WIMPs search, PRD 94, 0282006 (2016), arXiv:1607.07410 .
- Publication 2 : QF calibration for Silicon, 2017 JINST 12 P06014.

BROWN

Summary for DAMIC

- DAMIC CCDs have very low noise which is good for low mass WIMIP hunting. DAMIC has measured the quenching factor of silicon down to 100s keV recoil energy. A discrepancy comparing to the Lindhard model has been observed.
- All EFT $\mathcal{O}s$ have been studied and analyzed with DAMIC $\sim$ 0.6 kg*day data. No signal has been observed. 90% C.L. upper limits with have been set.
- We find the most sensitive EFT operators of WIMP-nuclear interaction, $\mathcal{O}_{11}$ for S.I. and $\mathcal{O}_{15}$ for S.D..
- Publication 1: WIMPs search, PRD 94, 0282006 (2016), arXiv:1607.07410 .
- Publication 2 : QF calibration for Silicon, 2017 JINST 12 P06014.

BROWN

outline

BROWN

LZ detector

- LZ: LUX (US) + ZEPLIN (UK).
- LUX: Large Underground Xenon experiment;
  ZEPLIN: ZonEd Proportional scintillation in LIquid Noble gases

LUX-ZEPLIN (LZ) detector

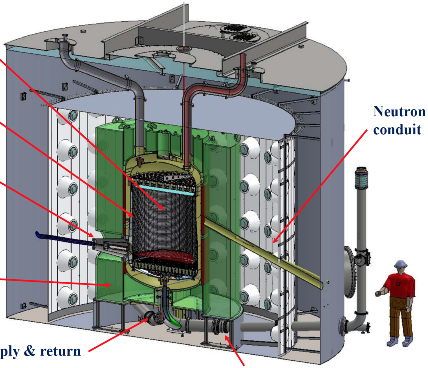

Technical Design Report, arXiv:1703.09144.

3

LZ Bkg

WIMP backgrounds summary

5.6 tonnes x 1000 days; ~1.5 to ~6.5 keV

Background Source	ER (cts)	NR (cts)
Detector Components	**9**	**0.07**
Surface Contamination	**40**	**0.39**
Laboratory and Cosmogenics	**5**	**0.06**
Xenon Contaminants	**819**	**0**
222Rn	681	0
220Rn	111	0
natKr (0.015 ppt g/g)	24	0
natAr (0.45 ppb g/g)	3	0
Physics	**322**	**0.51**
136Xe 2νββ	67	0
Solar neutrinos (pp+7Be+13N)	255	0
Diffuse supernova neutrinos	0	0.05
Atmospheric neutrinos	0	0.46
Total	1195	1.03
with 99.5% ER discrim., 50% NR eff.	**5.97**	**0.51**

LZ projected sensitivity

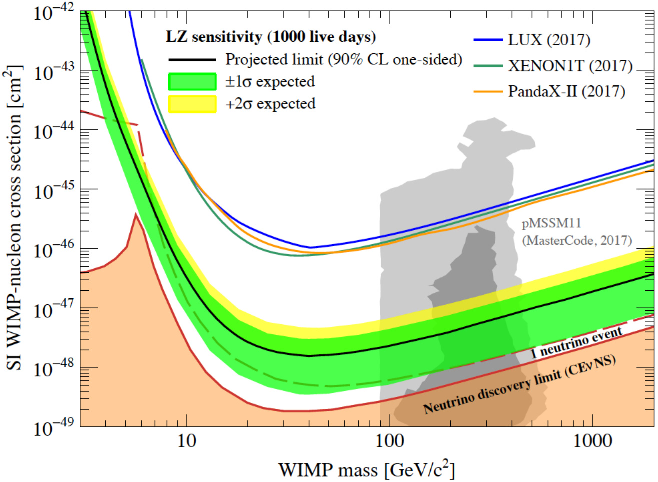

LZ members

LZ collaboration

38 institutions; 250 scientists, engineers, and technicians

1) IBS-CUP (Korea)
2) LIP Coimbra (Portugal)
3) MEPhI (Russia)
4) Imperial College London (UK)
5) Royal Holloway University of London (UK)
6) STFC Rutherford Appleton Lab (UK)
7) University College London (UK)
8) University of Bristol (UK)
9) University of Edinburgh (UK)
10) University of Liverpool (UK)
11) University of Oxford (UK)
12) University of Sheffield (UK)
13) Black Hill State University (US)
14) Brandeis University (US)
15) Brookhaven National Lab (US)
16) Brown University (US)
17) Fermi National Accelerator Lab (US)
18) Lawrence Berkeley National Lab (US)
19) Lawrence Livermore National Lab (US)
20) Northwestern University (US)
21) Pennsylvania State University (US)
22) SLAC National Accelerator Lab (US)
23) South Dakota School of Mines and Technology (US)
24) South Dakota Science and Technology Authority (US)
25) Texas A&M University (US)
26) University at Albany (US)
27) University of Alabama (US)
28) University of California, Berkeley (US)
29) University of California, Davis (US)
30) University of California, Santa Barbara (US)
31) University of Maryland (US)
32) University of Massachusetts (US)
33) University of Michigan (US)
34) University of Rochester (US)
35) University of South Dakota (US)
36) University of Wisconsin – Madison (US)
37) Washington University in St. Louis (US)
38) Yale University (US)

25

LZ timeline

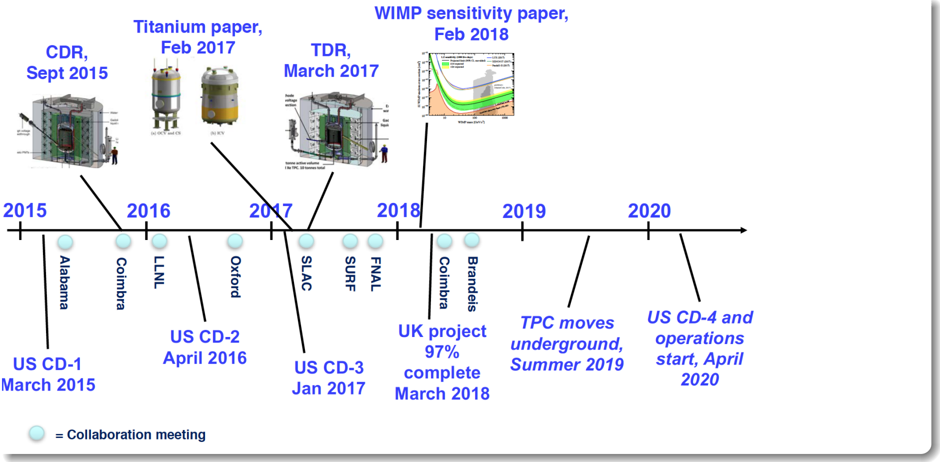
CDR,
Sept 2015
Titanium paper,
Feb 2017
TDR,
March 2017
WIMP sensitivity paper,
Feb 2018
2015
2016
2017
2018
2019
2020
Alabama
Coimbra
LLNL
Oxford
SLAC
SURF
FNAL
Coimbra
Brandeis
US CD-1
March 2015
US CD-2
April 2016
US CD-3
Jan 2017
UK project
97%
complete
March 2018
TPC moves
underground,
Summer 2019
US CD-4 and
operations
start, April
2020
= Collaboration meeting

outline

PMTs assembly at Brown

PMT dressing in Brown clean room (class 100)

Sector 1 PMT Dressing

Dressing fully completed within 3 hours, parts fit together smoothly

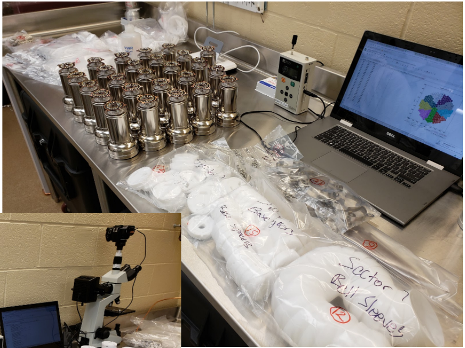

6

PMTs assembly at Brown

PMT assembly with a particle counter at the bottom of the PALACE, glass and PTFE slides monitoring dusts deposition

PALACE

Glass slides and PTFE slides both set up near the location of sector 1 during the whole exposure.

PTFE witness plates (exposed for sector 1 and will be shipped to SDSMT) and particle counters were placed at the bottom of PALACE interior

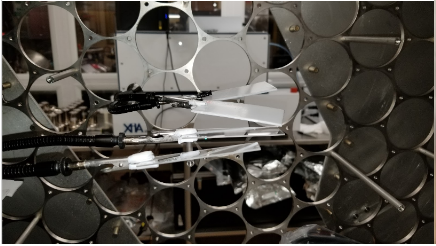

PMTs assembled on the bottom array at Brown

outline

Lowest calibration energy on LXe: understanding ^{8} neutrino Bkg events

- Deuterium-Deuterium (DD) generator generates (mono-E) 2.45 MeV neutrons isotropically, some hit the reflector, then reflected to the bar1 in the water tank.
- At a certain small angle, the E of reflected neutrons is tunable and mono-E. We set it to 160 degree and get 300 keV neutrons.
- Reflector material: in this simulation, EJ315 (CD); will change to LXe later.

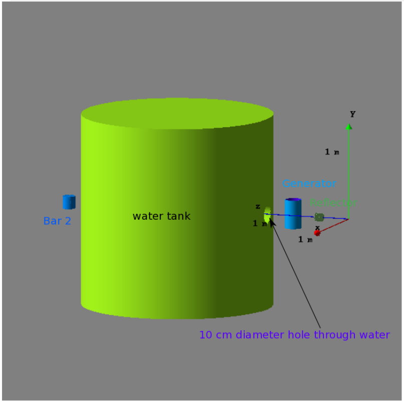

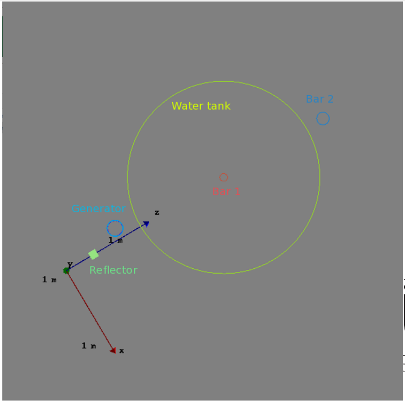

Preliminary simulation results

- We see the neutrons have two peaks, being scattered from C and D, respectively. Which demonstrates that we can use ToF to select interested 300 keV neutrons.

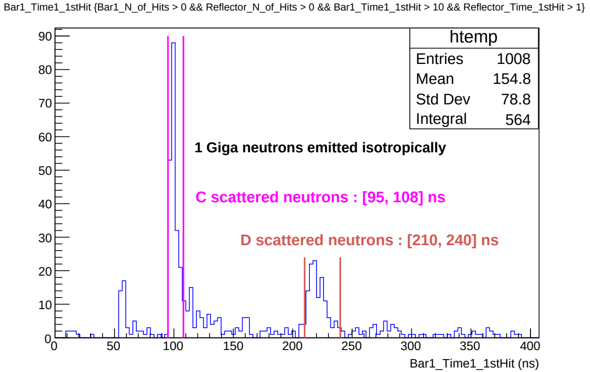

- A not novel but useful technique has been developed during the simulation: run high-statistic simulation on HPC, visualizing an interested event on a local PC with a unique pair of seeds numbers.

BROWN

Visualized trajectories on a local PC

- Left plot: The trajectory of an event having the Bar1_Time1_1stHit of 69 ns ($<$ 95 ns), turns out to be “accidental coincidence”: the neutron and it produced secondary particle(s) satisfy the cut condition.
- Right plot: The trajectory of an event having the Bar1_Time1_1stHit of 166 ns, slower than the population being scattered by C, faster than D, is double-scattering on C.

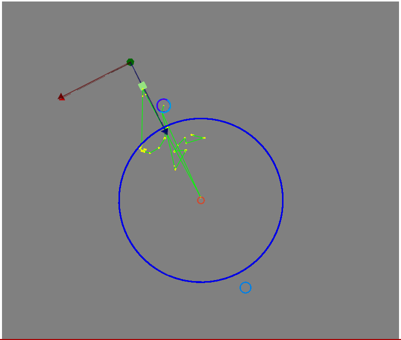

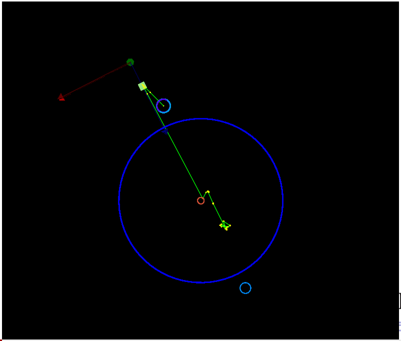

Visualized trajectories on a local PC

- Left plot: The trajectory of an event having the Bar1_Time1_1stHit of 225 ns ($210 < 225 < 240$), is an expected event: a 2.45 MeV neutron hits on the reflector once then being reflected to the Bar1 in the central place of the water tank.
- Right plot: The trajectory of an event having the Bar1_Time1_1stHit of 249 ns (> 240), slower than the population being scattered by D once, that is because the neutrons hits the water near the Bars first then being reflected to the Bar1.

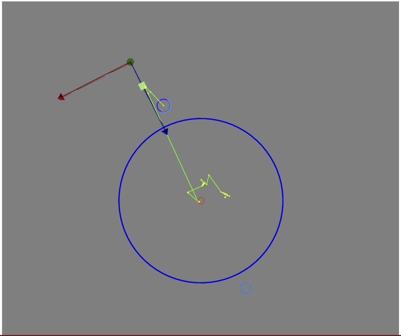

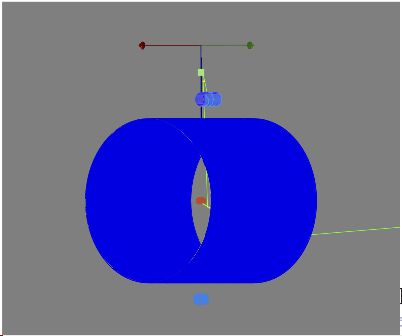

Tips for visualizing trajectories on a local PC

- To run on a HPC: you should have an executable file to run your simulation there, that means you don't need / want to recompile your scripts.
  (Working on a Brown HPC, we are able to submit 1000 jobs with $\sim$ 1 minute.)
- Seeds number can be only placed in particle generator; not Begin_of_event(), it's too late there.
- Be cautious to the possible repetitive events (that means N jobs = 1 job).
- We used the "systime()" which is the UNIX time of a machine as the source of seeds.
- The scripts run on a HPC and a local PC must be exactly the same, including the macro file(s).
- A paper has been submitted to JINST: JINST_027P_0718 (under review).

outline

Brief introduction on the LHC

Four main experiments of the LHC: ALICE, ATLAS, CMS, LHCb.

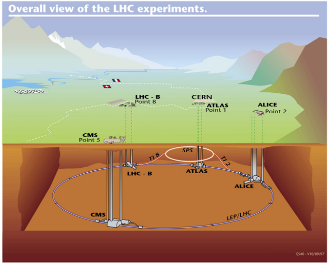

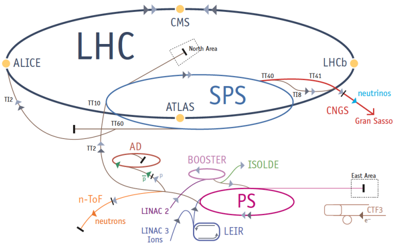

- LHC, Large Hadron Collider. 70 meters underground, Switzerland France board, close to Geneva. Length : 27 km.

  The LHC is the energy highest ever built machine.

Higgs is there !

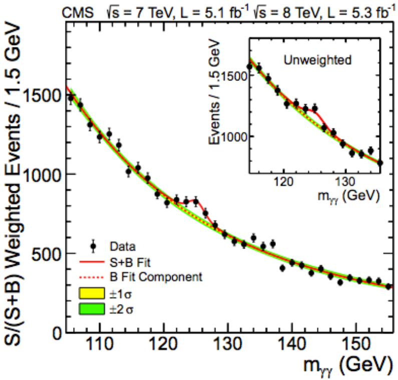

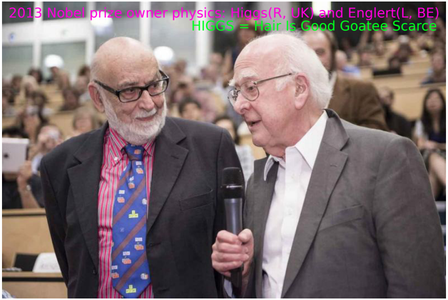

- The discovery of Higgs has been widely considered as the “biggest” moment in physics after the discovery of W,Z Boson in 1980s.

BROWN

outline

BROWN

What is GASTOF, Why we need it

GASTOF is “GAS Time Of Flight”. It’s a sub-10 ps time resolution gas Cherenkov detector. It’s one of the most important timing detectors for the FP420 and HPS (upgrade projects of ALTAS and CMS), stands for Forward Physics 420 (meters) and High Performance Spectrometer respectively.

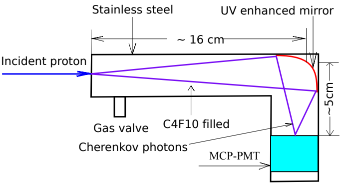

Two GasToF detectors used for beam test

- According to simulation, Cherenkov photons only contribute $\sim$ 2 ps, DAQ contributes $\sim$ 4 ps, so the time resolution of our detector system depends mainly on the one of MCP-MPT under the context of 10 ps timing.

BROWN

Cherenkov photons

- Cherenkov photons will be produced if a charged particle goes through a media with a velocity faster than the speed of light in this media. Just like a supersonic jet produces a sonic boom.
- GASTOF has been filled with 1.1 atm C_4F_{10}, the refraction index is 1.0014. The beam utilized in our beam test is 120 GeV Pion.

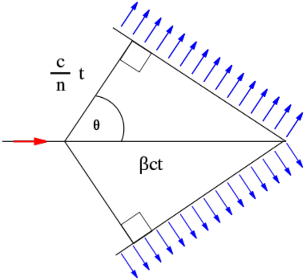

BROWN

Why we need GASTOF ? 1/2

Central exclusive channel [pXp]

The collision of p p results X (e^+e^-, Higgs etc) in a central detector (CMS, for instance) while two protons remain intact(lost less than 2% of their longitudinal momentum) flying back to back.

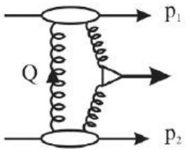

Central exclusive channel : signals and backgrounds

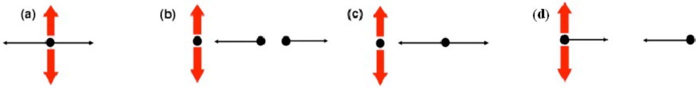

- (a) is a signal event, (b),(c) and (d) are background events.

Why we need GASTOF ? 2/2

GASTOF is supposed to improve the ratio of S/N (1 order or more).

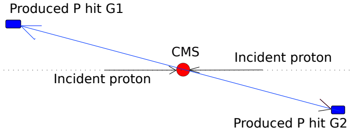

- Two GASTOF detectors will be put 220 meters away from the IP of CMS (ATLAS), $\sim$4-7 mm away from beam center.
- Imaging two "back-flying" protons arrived at two GasToFs with time variation $\Delta T = T_L - T_R$, assuming the two protons come from the same interaction, then the Z-position of this interaction could be obtained $Z_{pp} = 1/2 * \Delta T * c$ (c = the speed of light).
- The uncertainty of Z_{pp}, $\delta Z_{pp} = (c/\sqrt{2}) * \delta T$. $\delta T = 10$ ps $\Leftrightarrow$ $\delta Z_{pp} = 2.1$mm. The Z-position of the vertex related two protons, Z_{vertex}, could be obtained from a central detector ($\delta Z_{vertex} \approxeq 50$ μm).
- Finally, we require a match between Z_{pp} and Z_{vertex} to exclude (many) backgrounds.
- Better δT= better physics. 10 ps is the balance between physics benefit and current detector reachable performance.

outline

GASTOF charge measurement 1/2 - (MCP laser test)

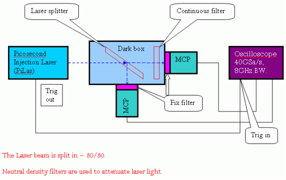

MCP-PMT laser test setup

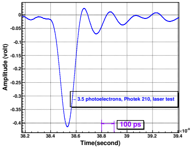

Typical signal of Photek 210 MCP measured with laser

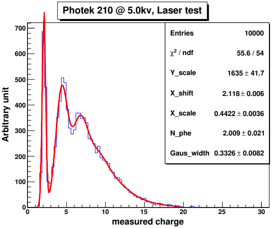

Charge measurement and fit (Photek 210)

$$Sum_0 = e^{-\mu} * [Gauss((x - x_{shift}) \cdot x_{scale},\ 0,\ \sigma_0)]$$

$$Sum_n = \sum_{n=1}^{N} \frac{e^{-\mu}}{n!} \mu^n * [Gauss((x - x_{shift}) \cdot x_{scale},\ n,\ \sqrt{n}\,\sigma_1)]$$

$$Fit\_function = y_{scale} \cdot (Sum_0 + Sum_n)$$

Charge fit function

GASTOF charge measurement 2/2 - (MCP beam test)

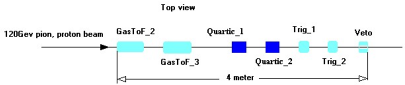

beam test setup

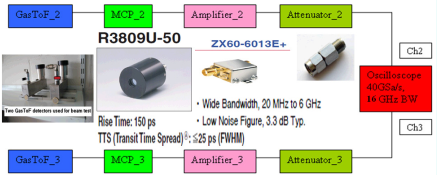

beam test detectors and DAQ

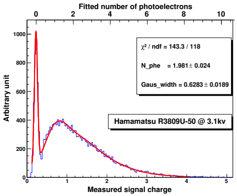

Charge fit (Hamamatsu R3809U-50)

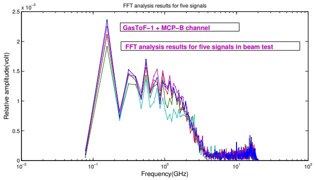

FFT analysis on typical signals of beam test

GASTOF time analysis 1/7, a couple of useful techniques

Technique 1 : signal reconstruction

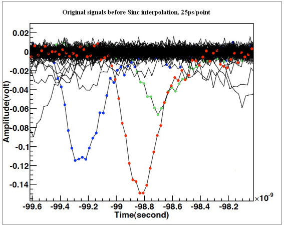

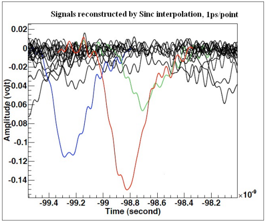

Technique 2 : CFD(Constant Fraction Discriminator) algorithm

- According to our analysis, comparing to “leading-edge timing + time walk correction”, CFD algorithm can result better time resolution and more events.

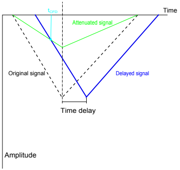

GASTOF time analysis 2/7: method 1

Time resolution obtained by “method 1”.

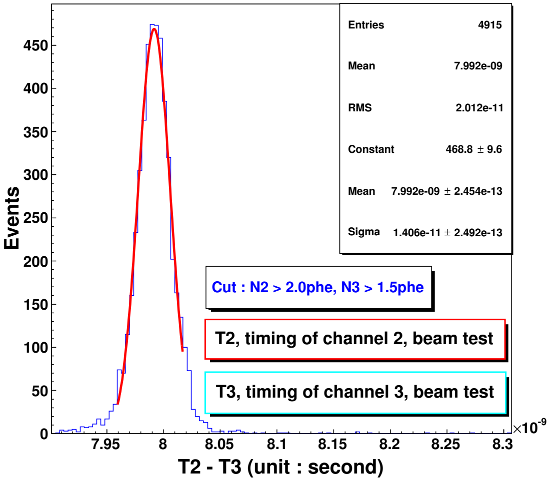

- Step 1 : Get the timing of two detectors with the CFD algorithm : T2 and T3.
- Step 2 : Get the histogram of “T2 - T3”.
- Step 3 : Get the sigma of above histogram with a Gaussian fit.
- From the left figure, the time resolution is 14.1 $\pm$ 0.25 ps(For two detectors)
- Next slides will explain how to figure out the time resolution of two detectors individually.

GASTOF time analysis 3/7 : method 2, motivation

The motivation of knowing individual time resolution

- The time resolution of an individual detector is more interesting.
- To do a crosscheck with the results of method 1 by an independent analysis method.
- To reach a deeper understanding on the performance of GASTOF detectors.

The basic of method 2 : Poisson statistics

- In our system : $\sigma^2 = \sigma_2^2/N_2 + \sigma_3^2/N_3$ (with same cut as method 1).
- σ is the time resolution of two detectors; σ_2 and σ_3 are "the time resolution per photoelectron" of each GASTOF separately ; N_2 and N_3 are the average number of phe of corresponding detectors.

BROWN

GASTOF time analysis 4/7 : method 2, figure out σ_i^2 VS $1/N_i$

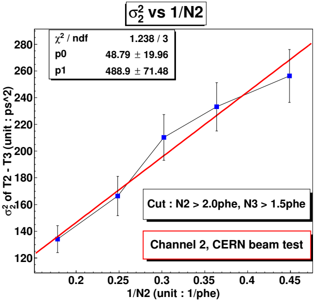

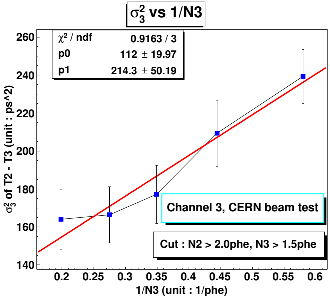

- In the left plot, the slope of a linear fit, “p1”, represents the time resolution per phe of GASTOF_2 : $\sim$ 22ps ($\sqrt{488.9}$).
- In the right plot, the slope of a linear fit, “p1”, represents the time resolution per phe of GASTOF_3 : $\sim$ 15ps ($\sqrt{214.3}$).

BROWN

GASTOF time analysis 5/7 : method 2, an example data point

$1/N_3$ in the range of [0.31,0.39]

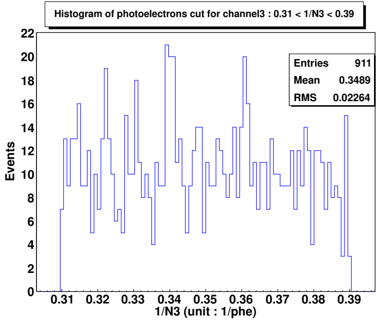

σ of T2 - T3 histogram with same cut

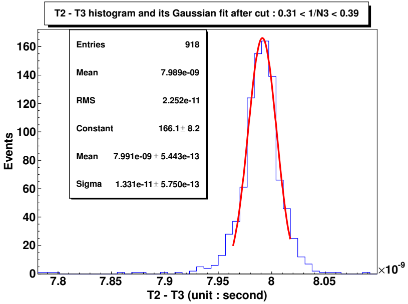

- As shown in the left plot, we select a charge interval of GASTOF3, get its mean value of 1/phe : 0.35. Using the cut of such a charge interval, we get a histogram of "T2-T3" then make a Gaussian fit to get $\sigma = 13.31$ps, as the right plot.
- "0.35" and $\sigma^2 = 13.31^2 = 177$ are the X and Y coordinates of the middle point of the right plot of previous slide.

BROWN

GASTOF time analysis 6/7 : method 2, average N_2 and N_3.

Average phe G2 : $N_2 = 3.6$

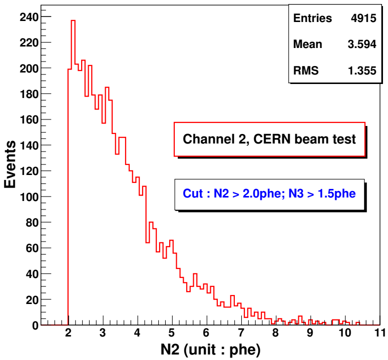

Average phe G3 : $N_3 = 3.2$

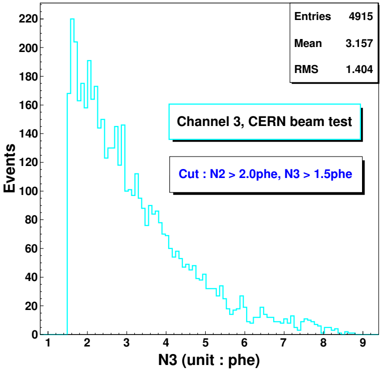

GASTOF time analysis 7/7 : method 2, very well consistent with method 1.

- Substitute the values obtained above, we get

$$\sqrt{\frac{\sigma_2^2}{N_2}+\frac{\sigma_3^2}{N_3}}=\sqrt{\frac{488.9\pm71.5}{3.6}+\frac{214.3\pm50.2}{3.2}}=14.2\pm0.89\ \ ps.$$

This is consistent very well with the result we obtained by method 1 : 14.1 ± 0.25 ps .

- Accordingly, we can get the time resolution of GASTOF_2 ,

$$\sigma_{ch2}=\sqrt{\frac{\sigma_2^2}{N_2}}=\sqrt{\frac{488.9\pm71.5}{3.6}}=11.7\pm0.85\ \ ps$$

And GASTOF_3,

$$\sigma_{ch3}=\sqrt{\frac{\sigma_3^2}{N_3}}=\sqrt{\frac{214.3\pm50.2}{3.2}}=8.2\pm0.96\ \ ps$$

Summary on GasToF

Summary

- Very good understanding on charge and timing for GASTOF detector.
- (Sub-)10 ps time resolution has been achieved: $\sigma \sim$ = 8 and 12 ps .
  Best time resolution among similar gas detectors ever since.
- A relation of "σ^2/N_{phe}" has been figured out for both detectors.
- Paper: NIM(A) 762 (2014) 77-84.

Outlook

- Strategies to increase GASTOF's time resolution.
  (1) Increasing the number of photoelectrons.
  (2) Increasing the rise time of signals.
  After the application of above improvements, we've expected to get $\sim$5 ps time resolution(σ).
- The efficiency of GASTOF detectors should be studied further.
- The life of MCP. For instance, using SiPM(Of course, one of the drawbacks is that SiPM has a worse noise than MCP).

Thanks